(Received 11 June 2025, Accepted 14 July 2025, Scheduled 24 July 2025)

Wideband Antenna Design with Notched Flower Shaped Patch for Wireless Applications

Bharat D. Prajapati[1, 3, *], Bhavesh Jaiswal[2], and Pravin J. Dalvadi[3]

[1] *Monark University, Gujarat, India*
[2] *Electronics & Communication Engg. Department, Hasmukh Goswami College of Engineering, Gujarat, India*
[3] *Electronics & Communication Engg. Department, Government Polytechnic College, Gandhinagar, India*

ABSTRACT: A notched flower-shaped patch wideband MPA antenna is designed with defected ground (DGS) to realize magnified performance for the various wireless applications. The several modes effectively excited in antenna and also higher order modes merging efficiently to enable wider impedance bandwidth. The current distribution is improved with a notched flower-shaped patch and efficient stimulation of multiple modes, while the enhanced impedance matching and extension of bandwidth are contributed with defective ground. The antenna has overall size measuring length of 1.14λ, width of 1.14λ, and height of 0.04λ. The result exhibits a return loss lower than -10 dB across 5.12 GHz to 8.58 GHz, with 5.58 dB peak gain. This range supports wide range of wireless applications, such as Wi-Fi 6/6E, Sub-6 GHz 5G NR, short range automative radar, and C-band satellite communication. The compact size makes it appropriate for integration on space constrained device.

1. INTRODUCTION

Microstrip patch antennas (MPAs) are widely used in various modern wireless communication applications due to their miniaturized and low profile. In a present time, research is enhancing characteristic performance and overcoming inherent constraint [2, 10, 22]. A series fed novel patch-array operating at 5.8 GHz addressing bandwidth (BW) limitations and huge sidelobe levels, critical for various radar applications is presented [1]. Miniaturized designed arrays for Industrial, Scientific, and Medical (ISM) and internet of things (IoT) bands, integrating specific techniques to improve key parameter performance while lowering overall size of antenna are explored [3]. A UWB patch antenna design, utilizing and incorporating a single circular element with a borosilicate glass substrate to acquire wider frequency operation is presented [4].

Bandwidth enhancement techniques, concentrating on the implementation of shorting-vias and parasitic patches, are investigated [5]. A gain improved MPA that incorporates repeated rampart-line to alter an effective dielectric constant is presented [6]. An antenna design challenge for small volume which exactly covers Wi-Fi 6 unbalanced spectrum is covered [7]. The MPA with high directivity, based on modified TM modes-odd, appropriate for LOS (line-of-sight) communication areas is investigated [8]. A small, miniaturized, wideband elastomeric textile patch antenna integrated with an artificial magnetic conductor (AMC) for various medical, IoT, and other applications is introduced [9]. This analysis collectively pointing present day advancement in microstrip antenna technology, driven by various requirement of growing wireless communication systems. Defected ground structure (DGS) is used to improve patch antenna performance by reducing surface wave effects, changing flow of current, and improving impedance matching, which broadly lead to bandwidth enhancement [2, 3, 22]. A geometry of elliptical patch antenna with asymmetric axes enables broader operation bandwidth, improved radiation characteristic and reduces surface wave losses due to curved edges. By adjusting its axes, it can also be optimized for wideband performance. Nonuniform axes of elliptical patches exhibit modes excitation, which improve antenna performance [2, 9, 10, 22].

The proposed antenna structure energized via a microstrip feedline employs an elliptical inclined patch, longitudinally symmetric on a dielectric substrate. A DGS utilizes strategically circular and rectangular slots to optimize radiation gain, BW (impedance bandwidth), and also reduces cross-polarized fields. This antenna provides a broad operation BW (bandwidth) of 3.46 GHz, spanning from 5.12 to 8.58 GHz. Analysis of a radiation pattern indicates bidirectional and omnidirectional radiation characteristics in E and H planes accordingly. Extensive parametric analysis and simulated surface current distribution are performed to assess and fine-tune the antenna's electromagnetic behavior.

2. PROPOSED ANTENNA DESIGN

Figure 1 presents a structural layout and dimensional specifications of an antenna design. The antenna employs longitudinally symmetry, configured in plane (x-y). The structure consists of a central radiating elliptical patch united with an inclined elliptical sub patch ($E2$, $E3$ at $20°$, $-20°$ & $E4$, $E5$ at $40°$, $-40°$), with defined semi-major & semi-minor axes. An elliptical slot (R_{pc}) and a microstrip feed line, dimensioned by

* Corresponding author: Bharat D. Prajapati (bharatdprajapati@gmail.com).

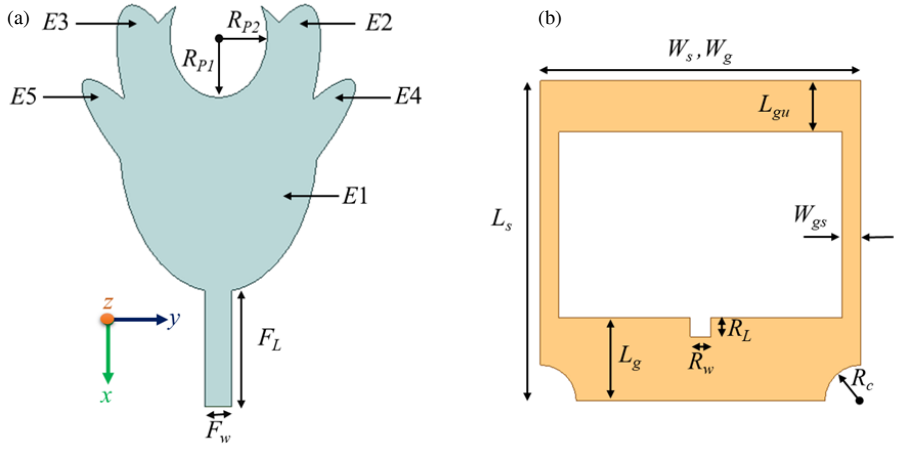

FIGURE 1. Optimized antenna design: (a) Top view, (b) Bottom view.

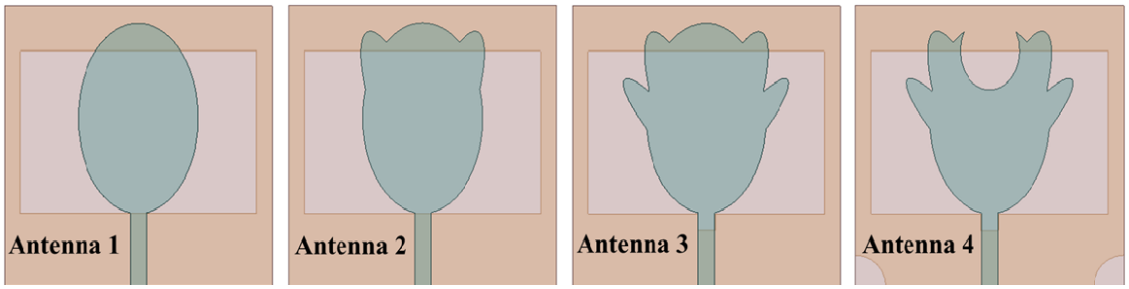

FIGURE 2. Progressive evaluation of antenna.

its length (E_{fl}) and width (E_{fw}) are implemented on the upper part of a dielectric substrate.

The substrate is characterized by 1.6 mm thickness, 4.4 ε_r (relative permittivity), and 0.02 loss tangent. A DGS is etched into bottom layer of the substrate to improve key performance parameters, radiation gain, BW, and the suppression of cross-polarization components.

The ground plane incorporates a wide rectangular slot and an additional rectangular notch, both defined by their respective lengths and widths. Furthermore, a pair of symmetrically placed circular parasitic slots (radius R_{gc}) are embedded near the ground plane's corners. The physical dimension is $1.14\lambda \times 1.14\lambda \times 0.04\lambda$. Detailed structural parameters are listed in Table 1.

TABLE 1. Parameter values of design.

Parameter	Value	Parameter	Value
$E1$ (Semi major axis)	0.39λ	F_w	0.07λ
$E1$ (Semi minor axis)	0.26λ	W_s, W_g	1.14λ
$E2$, $E3$ (Semi major axis)	0.39λ	L_s	1.14λ
$E2$, $E3$ (Semi minor axis)	0.1λ	L_g	0.3λ
$E4$, $E5$ (Semi major axis)	0.27λ	L_{gu}	0.18λ
$E4$, $E5$ (Semi minor axis)	0.06λ	W_{gs}	0.07λ
R_{P1}	0.16λ	R_L	0.07λ
R_{P2}	0.13λ	R_w	0.07λ
F_L	0.3λ	R_c	0.13λ

3. ANTENNA DESIGN EVOLUTION AND PERFORMANCE PARAMETER ANALYSIS

As outlined in Figure 2, the antenna geometry is progressively modified to support multiple resonant modes for wideband performance. In Antenna 1, the design consists of a basic elliptical patch that offers limited bandwidth. In Antenna 2, two inclined elliptical shapes are symmetrically integrated with the base structure, extending the surface current paths and enabling the excitation of higher-order resonances. Antenna 3 further adds two additional inclined ellipses and introduces a rectangular slot in the ground plane, which supports additional resonances and improves impedance matching. In Antenna 4, an elliptical notch is embedded in the patch, and a circular cut is incorporated in the ground plane, allowing further tuning of resonances and enhancing the coupling mechanism. This progressive geometric evolution significantly improves impedance characteristics and broadens the operational bandwidth through the activation of TM_{10} and higher-order modes.

In Figure 3, S_{11} characteristics show a clear enhancement in impedance matching and bandwidth as the antenna design progresses through successive modifications. Initially, the reflection coefficient curve exhibits a single narrow resonance with relatively shallow depth, indicating limited bandwidth. With the first structural enhancement, an additional resonance emerges, and the return loss deepens significantly, indicating improved impedance matching. Further geometric evolution introduces more pronounced notches in the S_{11} curve, result-

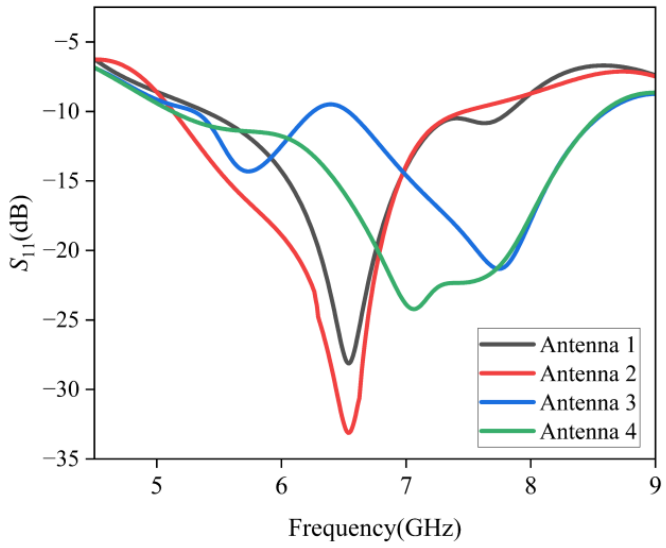

FIGURE 3. Return loss variation across diverse designs.

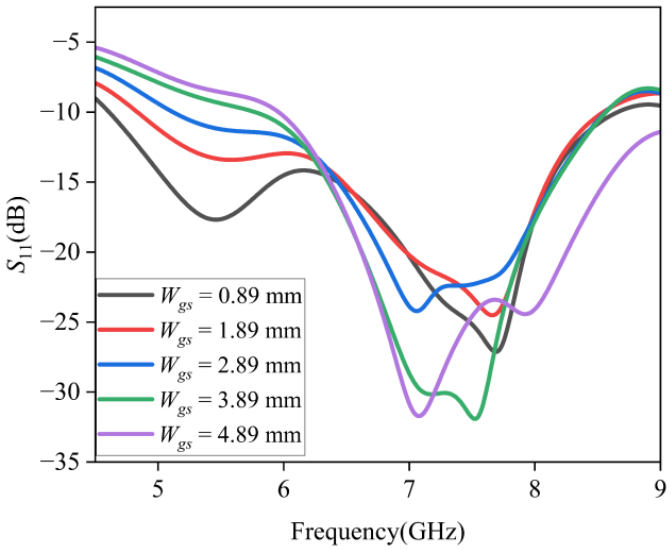

FIGURE 4. Return loss variation relative to changes in side ground strip width (W_{gs}).

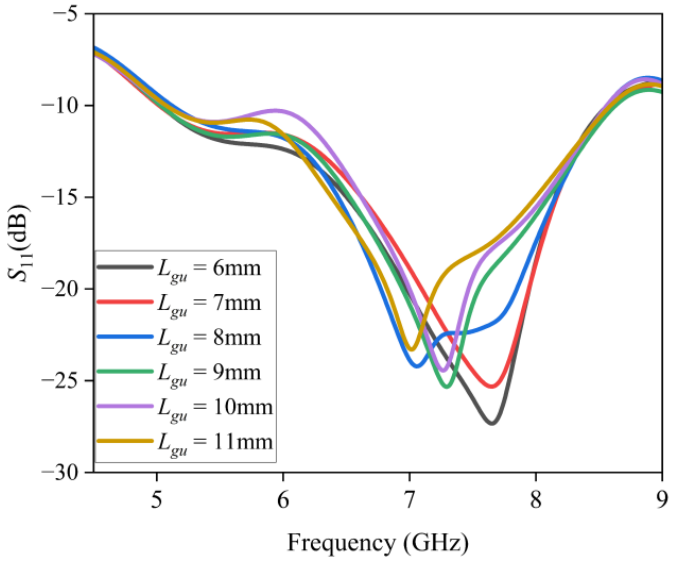

FIGURE 5. Return loss variation relative to changes in upper ground strip length (L_{gu}).

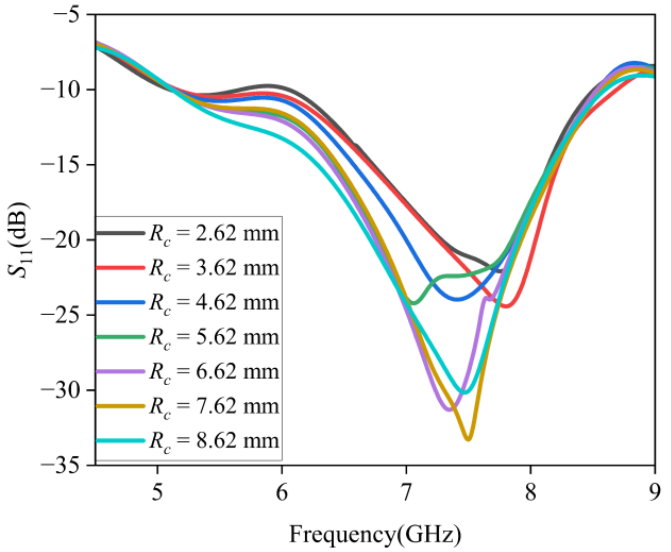

FIGURE 6. Variation in return loss as a function of ground plane circular slot radius (R_c).

ing in a wider bandwidth and multiple well-defined resonant points. In the final configuration, the reflection coefficient displays a broad frequency range, confirming effective impedance tuning and wideband performance due to the cumulative design enhancements.

Figure 4 shows that varying the width (W_{gs}) significantly affects the antenna's return loss, with wider slots enhancing impedance matching and bandwidth. Optimal performance, marked by deeper and multiple resonant dips, occurs at W_{gs} values of 2.89 mm and 3.89 mm, indicating more efficient energy coupling.

As depicted in Figure 5, increasing L_{gu} from 6 mm to 8 mm improves bandwidth by shifting the -10 dB cutoff frequencies outward, with $L_{gu} = 8$ mm providing the widest and most stable frequency range. Beyond 8 mm, the cutoff frequencies shift inward, and the return loss becomes less uniform, indicating reduced bandwidth and performance.

Figure 6 illustrates the impact of R_c variation on -10 dB return loss bandwidth, highlighting its role in tuning antenna performance. Increasing R_c from 2.62 mm to 7.62 mm substantially enhances bandwidth due to improved resonant coupling. Beyond 7.62 mm, bandwidth improvement saturates, indicating an optimal geometrical threshold.

The impact of R_L on BW is evident from the S_{11} response across different R_L values depicted in Figure 7. As R_L varies from 1.5 mm to 4 mm, a -10 dB bandwidth widening indicates improved impedance matching. The widest bandwidth and deepest resonance occur at $R_L = 3$, 3.5 mm, showing optimal performance. Overall, increasing R_L enhances bandwidth, with a slight downward shift in resonant frequency.

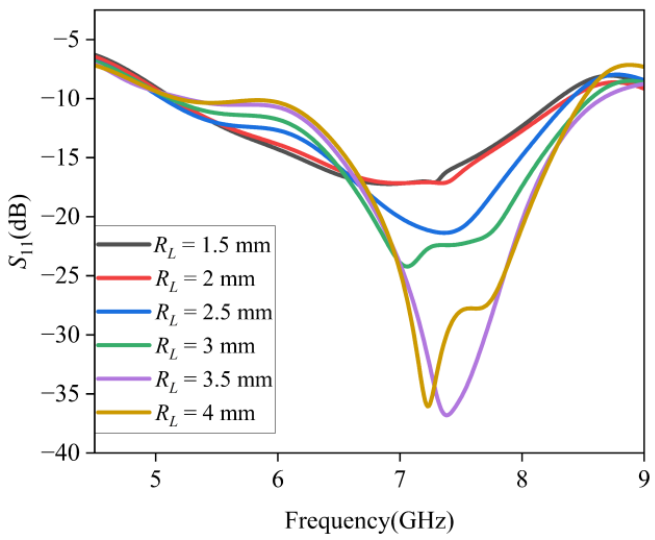

FIGURE 7. S_{11} variation as a function of ground plane rectangle slot length (R_L).

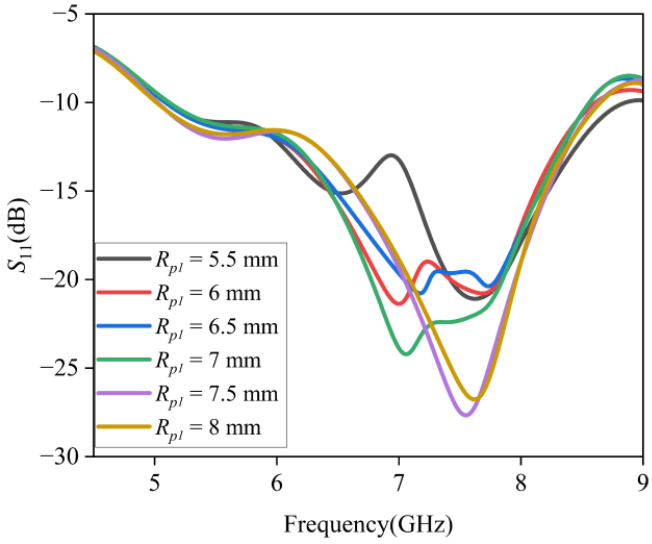

FIGURE 8. Impact of patch elliptical slot major length (R_{p1}) on S_{11}.

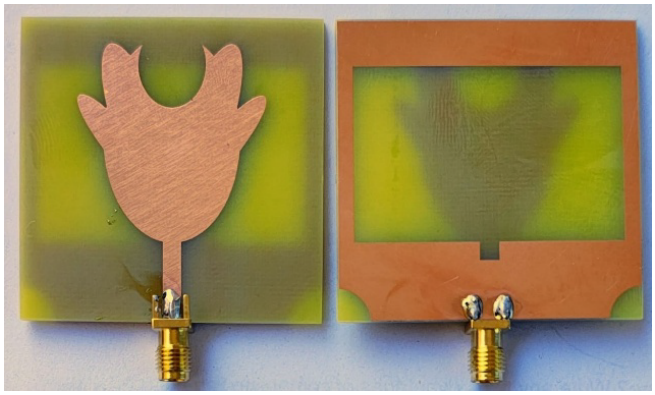

FIGURE 9. Prototype antenna.

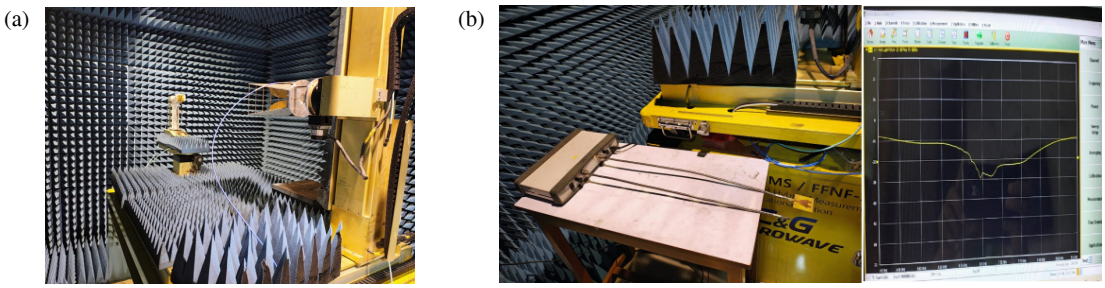

FIGURE 10. (a), (b) Measurement setup of the proposed antenna inside the anechoic-chamber.

Figure 8 delineates R_{p1} impact on impedance bandwidth. As R_{p1} is incremented, the reflection coefficient demonstrates pronounced minimization, and the corresponding bandwidth exhibits substantial augmentation, signifying enhanced impedance congruence. The most profound resonance and maximal bandwidth expansion occur notably at R_{p1} values of 7 mm to 8 mm. Consequently, increasing R_{p1} facilitates superior bandwidth characteristics and optimal return loss performance.

4. RESULTS AND DISCUSSION

Figure 9 shows the proposed antenna prototype. The suggested MPA is simulated using High Frequency Structure Simulator (HFSS), and the fabricated MPA is tested in an anechoic chamber, depicted in Figure 10. The analysis examines the return loss, radiation pattern, gain, and voltage standing wave ratio (VSWR), comparing the measured results with the simulation data.

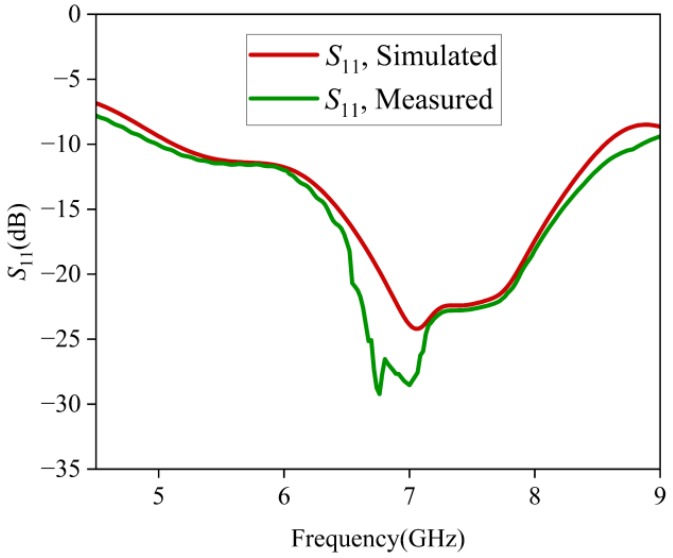

FIGURE 11. S_{11} parameter: simulated vs. measured results.

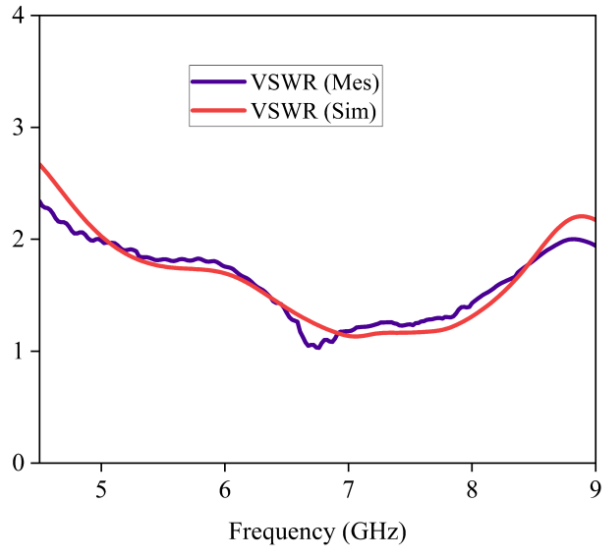

FIGURE 12. VSWR performance: simulation and measurement.

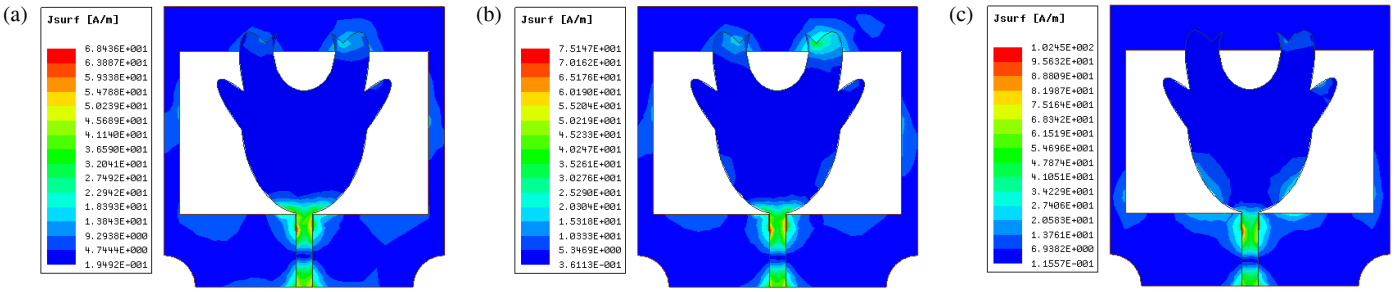

FIGURE 13. Current distribution analysis of the proposed antenna. (a) 6.7 GHz, (b) 7 GHz, & (c) 8.1 GHz.

TABLE 2. The comparative analysis of the proposed antenna with documented antenna designs.

Ref.	Size	Frequency Range (GHz)	BW (%)	Substrate	Technique-Feeding	Gain (Peak)
[11]	$0.64\lambda\times0.64\lambda\times0.12\lambda$	4.7–7.35	44	Rogers RO4003	Probe	7.2 dBi
[12]	$0.87\lambda \times 0.87\lambda \times 0.02\lambda$	4.83–8.17	50.2	FR4	Microstrip	5.2 dBi
[13]	$0.88\lambda\times0.88\lambda\times0.05\lambda$	4.25–6.27	38.4	Rogers RO4350B	Microstrip	6.85 dBi
[14]	$0.87\lambda \times 0.87\lambda \times 0.12\lambda$	4.65–7.21	43.2	Rogers Duroid 5880	Coaxial	8 dBic
[15]	$0.75\lambda \times 0.75\lambda \times 0.08\lambda$	4.69–6.52	30	RT/Duroid 5880	Microstrip	6 dBi
[16]	$0.47\lambda \times 0.47\lambda \times 0.07\lambda$	4.3–5.8	29.7	FR4	Microstrip	5.6 dBic
[17]	$1.08\lambda \times 1.08\lambda \times 0.03\lambda$	4.81–6.01	22.18	Rogers RO4003C	Probe	5.06 dBi
[18]	$0.57\lambda \times 0.57\lambda \times 0.05\lambda$	7.23–9.82	30.4	Rogers 4350B	Probe	5 dBi
[19]	$0.58\lambda \times 0.55\lambda \times 0.03\lambda$	5.25–5.95	12.5	Rogers 5870	Coaxial	4.95 dBi
[20]	$0.4\lambda \times 0.39\lambda \times 0.02\lambda$	3.4–4.3	23.4	FR4	Probe	3 dBi
Present Work	$1.14\lambda \times 1.14\lambda \times 0.04\lambda$	5.12–8.58	50.51	FR4	Microstrip	5.58 dB

Figures 11 & 12 illustrate the comparison of simulated and measured S_{11} (reflection coefficient) and VSWRs across the frequency spectrum. The results exhibit strong correlation and consistency. The proposed antenna successfully achieves a BW of 3.46 GHz (50.51%), spanning a frequency range of 5.12–8.58 GHz while maintaining an S_{11} value below -10 dB.

Figure 13 illustrates surface current patterns at 6.7 GHz, 7 GHz, and 8.1 GHz, showing how the antenna excites different resonant modes. Current begins near the feed and gradually extends along the arms and edges, forming intricate paths. These variations suggest the activation of higher-order modes, improving radiation characteristics. The growing current strength

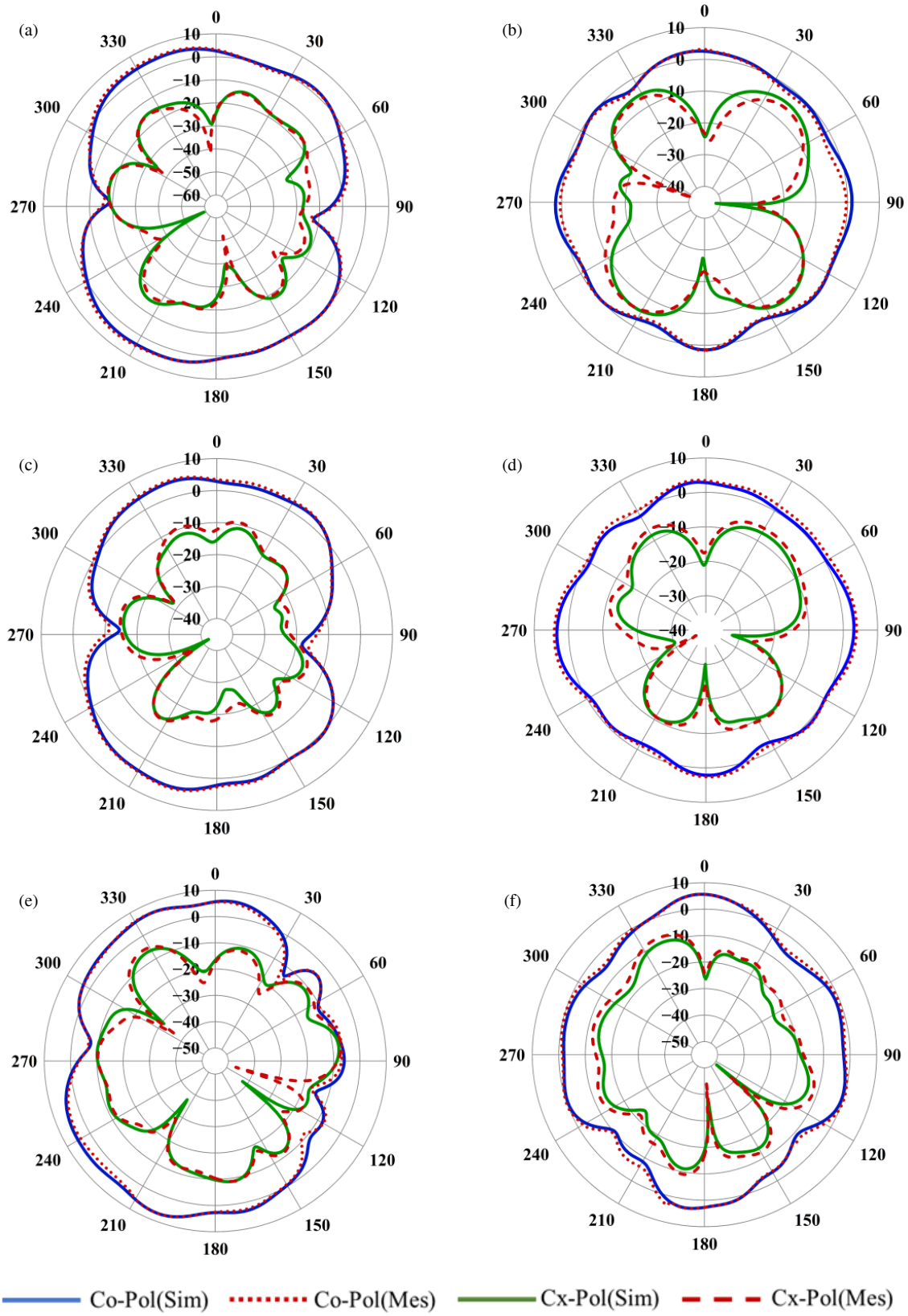

FIGURE 14. Radiation patterns, far field of the designed antenna, measured & simulated: (a) 6.7 GHz, E-field, (b) 6.7 GHz, H-field, (c) 7 GHz, E-field, (d) 7 GHz, H-field, (e) 8.1 GHz, E-field, (f) 8.1 GHz, H-field.

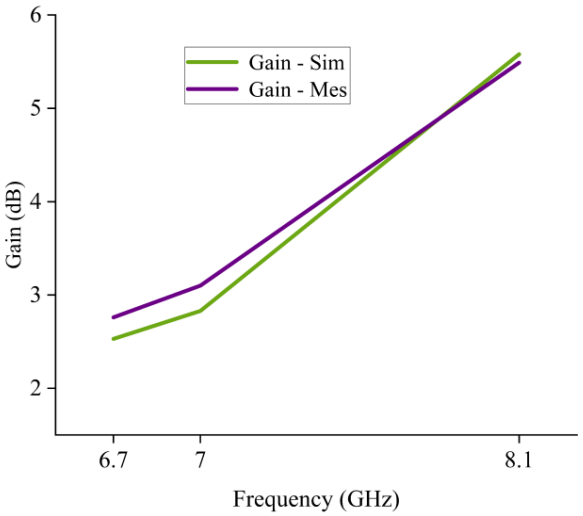

FIGURE 15. Measured and simulated gains of the designed antenna.

and spread confirm the antenna's effective broadband operation and high efficiency.

Figure 14 illustrates radiation patterns, far field in both E-plane (XZ-plane, $\Phi = 0°$) and H-plane (YZ-plane, $\Phi = 90°$) for a proposed antenna at frequencies of 6.7, 7, and 8.1 GHz. In the XZ plane, the pattern reveals a clear bidirectional nature, which aids in focused signal transmission. On the other hand, the YZ plane shows a near-omnidirectional pattern, ensuring wider coverage and reliable performance.

Table 2 compares the performance of proposed antenna with other reported designs, assessing key parameters such as physical dimensions, gain, BW (%), substrate materials, frequency range, radiation efficiency, and feeding methods. Figure 15 displays the measured gains of 2.76 dB, 3.1 dB, and 5.58 dB for the designed antenna at various frequency points.

5. CONCLUSION

A notched flower-shaped wideband MPA with defective structure of ground is presented. The radiation mode is energized by microstrip line feeding, which enhances the bandwidth of presented design. It exhibits a return loss lower than -10 dB across 5.12 GHz to 8.58 GHz frequency range and a bandwidth of 3.46 GHz (50.51%). In the entire frequency span, the VSWR is lower than 2 with 5.58 dB of maximum gain. The presented antenna is suitable for various applications.

ACKNOWLEDGEMENT

We would like to thank Entuple Technologies Pvt. Ltd., Ahmedabad, Gujarat, India for providing a measurement support.

REFERENCES

[1] Sacco, G., P.D'Atanasio, and S. Pisa, "A wideband and low-sidelobe series-fed patch array at 5.8 GHz for radar applications," *IEEE Antennas and Wireless Propagation Letters*, Vol. 19, No. 1, 9–13, Jan. 2020.

[2] Balanis, C. A., *Antenna Theory: Analysis and Design*, John Wiley & Sons, 2016.

[3] Olan-Nuñez, K. N., R. S. Murphy-Arteaga, and E. Colín-Beltrán, "Miniature patch and slot microstrip arrays for IoT and ISM band applications," *IEEE Access*, Vol. 8, 102 846–102 854, 2020.

[4] Seng, T. K., T. K. Geok, H. A. Ghani, C. J. Kit, and L. L. Hong, "Microstrip antenna design for ultra-wideband frequency," in *2017 International Conference on Robotics, Automation and Sciences (ICORAS)*, 1–5, Melaka, Malaysia, 2017.

[5] Xu, K. D., H. Xu, Y. Liu, J. Li, and Q. H. Liu, "Microstrip patch antennas with multiple parasitic patches and shorting vias for bandwidth enhancement," *IEEE Access*, Vol. 6, 11 624–11 633, 2018.

[6] Chen, X., Y. Wei, Y. Li, Z. Liang, S. Y. Zheng, and Y. Long, "A gain-enhanced patch antenna with a periodic microstrip rampart line," *IEEE Open Journal of Antennas and Propagation*, Vol. 3, 83–88, 2022.

[7] Gao, S., L. Chang, A. Zhang, Y. Li, and Z. Zhang, "Small-volume microstrip patch antennas exactly covering Wi-Fi 6 bands of 2.4-2.5 GHz and 5.15-5.85 GHz," *IEEE Transactions on Antennas and Propagation*, Vol. 71, No. 7, 5739–5748, Jul. 2023.

[8] Anguera, J., A. Andújar, and J. Jayasinghe, "High-directivity microstrip patch antennas based on TModd-0 modes," *IEEE Antennas and Wireless Propagation Letters*, Vol. 19, No. 1, 39–43, Jan. 2020.

[9] Dey, A. B., S. Kumar, W. Arif, and J. Anguera, "Elastomeric textile substrates to design a compact, low-profile AMC-based antenna for medical and IoT applications," *IEEE Internet of Things Journal*, Vol. 10, No. 6, 4952–4969, Mar. 2023.

[10] Prajapati, B. D. and B. Jaiswal, "Comprehensive analysis of microstrip patch antenna for wireless application," *Indian Journal of Natural Sciences*, Vol. 15, No. 87, 6901–6911, Dec. 2024.

[11] Chatterjee, J., A. Mohan, and V. Dixit, "Broadband circularly polarized h-shaped patch antenna using reactive impedance surface," *IEEE Antennas and Wireless Propagation Letters*, Vol. 17, No. 4, 625–628, Apr. 2018.

[12] Ding, Z., D. Zhang, and C. Ma, "Broadband antenna design with integrated CB-CPW and parasitic patch structure for WLAN, RFID, WiMAX, and 5G applications," *IEEE Access*, Vol. 8, 42 877–42 883, 2020.

[13] Cheng, B., Z. Du, and D. Huang, "A differentially fed broadband multimode microstrip antenna," *IEEE Antennas and Wireless Propagation Letters*, Vol. 19, No. 5, 771–775, May 2020.

[14] Ding, K., Y. Wu, K.-H. Wen, D.-L. Wu, and J.-F. Li, "A stacked patch antenna with broadband circular polarization and flat gains," *IEEE Access*, Vol. 9, 30 275–30 282, 2021.

[15] García-Alcaide, N., A. Fernández-Prieto, R. R. Boix, V. Losada, J. Martel, and F. Medina, "Design of broadband aperture-coupled stacked microstrip antennas using second-order filter theory," *IEEE Transactions on Antennas and Propagation*, Vol. 70, No. 7, 5345–5356, Jul. 2022.

[16] Zheng, B., N. Li, X. Li, X. Rao, and Y. Shan, "Miniaturized wideband CP antenna using hybrid embedded metasurface structure," *IEEE Access*, Vol. 10, 120 056–120 062, 2022.

[17] Zhang, Y. and Y. Li, "Wideband microstrip antenna in small volume without using fundamental mode," *Electromagnetic Science*, Vol. 1, No. 2, 1–6, Jun. 2023.

[18] Li, D., B. Yu, W. Li, X. Zhu, and X. Yuan, "Broadband integrated differentially fed patch antenna with tightly coupled elements," *IEEE Antennas and Wireless Propagation Letters*, Vol. 22, No. 10, 2457–2461, Oct. 2023.

[19] Kumari, P. and S. Das, "A wideband circularly polarized SIW MIMO antenna based on coupled QMSIW and EMSIW resonators for sub-6 GHz 5G applications," *IEEE Antennas and Wireless Propagation Letters*, Vol. 23, No. 10, 2979–2983, Oct. 2024.

[20] Qian, L., X. Chen, X. Liu, H. Zhou, H. Wang, and M. Hou, "Low-profile wideband patch antenna using even and odd modes for 5G terminal applications," *IEEE Antennas and Wireless Propagation Letters*, Vol. 23, No. 8, 2476–2480, Aug. 2024.

[21] Kumar, G. and K. P. Ray, *Broadband Microstrip Antennas*, Artech House, 2003.

[22] Prajapati, B. D., B. Jaiswal, and P. J. Dalvadi, "Wideband elliptical patch antenna integrating a circular notch and defected ground structure," *Progress In Electromagnetics Research C*, Vol. 156, 161–168, 2025.